Supplementary Figures

Zeeman Effect on Surface Electron Transport in Topological Insulator Bi_2Se_3 Nanoribbons

Li-Xian Wang,[a, †] Yuan Yan,[a, †] Liang Zhang,[a, †] Zhi-Min Liao,[a, b *] Han-Chun Wu,[c *] Da-Peng Yu[a, b]

[a]State Key Laboratory for Mesoscopic Physics, Department of Physics, Peking University, Beijing 100871, P.R. China

[b]Collaborative Innovation Center of Quantum Matter, Beijing, P.R. China

[c]School of Physics, Beijing Institute of Technology, Beijing, 100081, P.R. China

[†]These authors contributed equally to this work.

* e-mail: liaozm@pku.edu.cn (ZML); wuhc@bit.edu.cn (HCW).

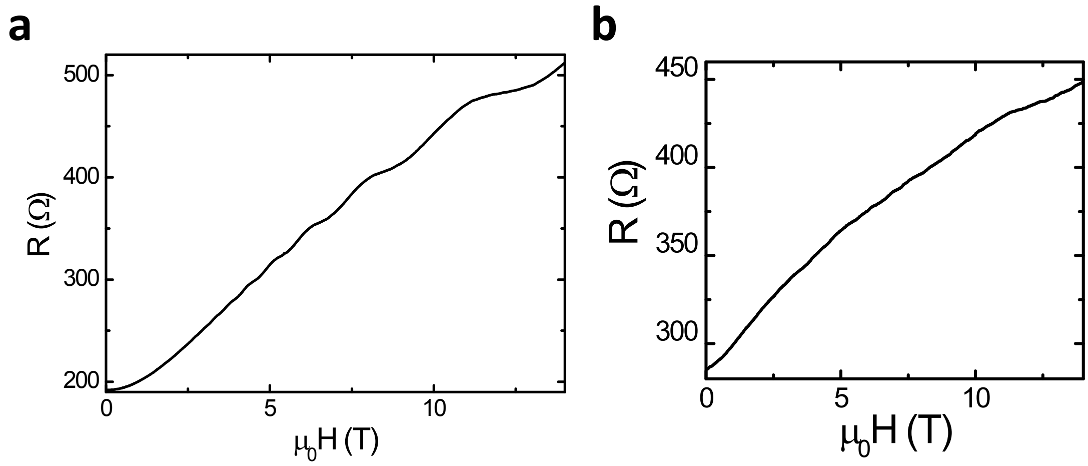

Supplementary Figure S1. Magnetoresistance of a Bi_2Se_3 nanoribbon measured at 1.5 K for (a) the first round and (b) the second round after the sample was took out from the cryostat and then was put into the cryostat again. The significantly decreased SdH oscillations can be understood as follow, which supports the surface origin of the oscillations. Water drops were found on the sample surface after it was taken out for a while, which may greatly degrade the surface quality and lower down the carrier mobility of surface states, despite of the robustness of topologically protected surface states.

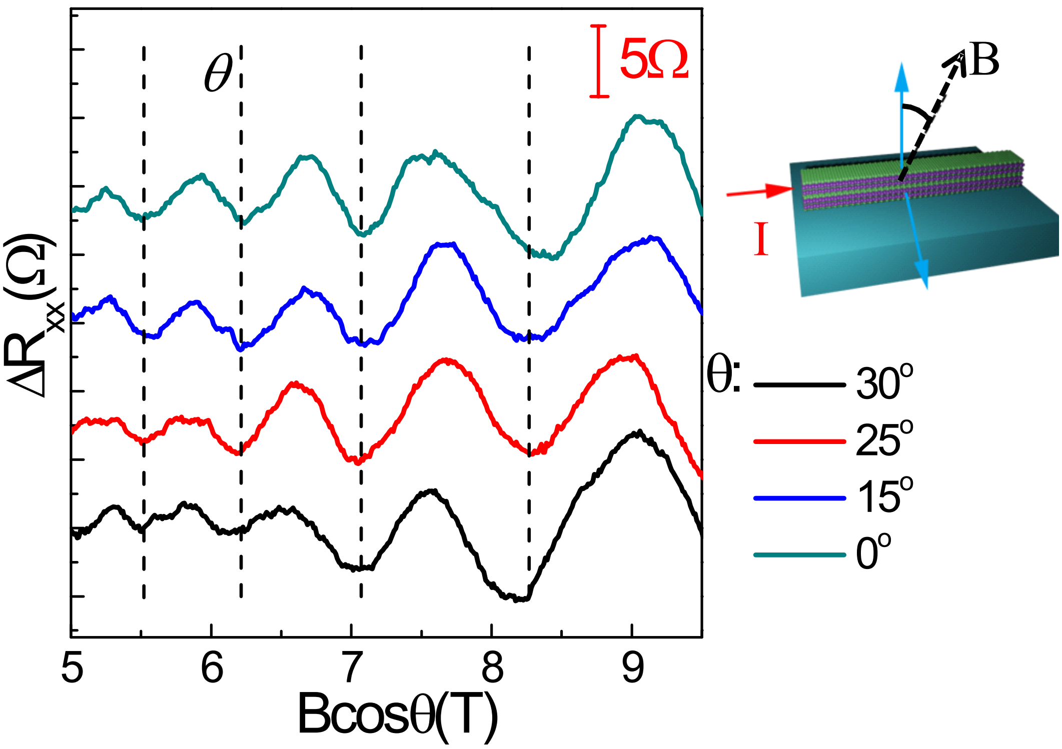

Supplementary Figure S2. Shubnikov–de Haas oscillations ΔR as a function of $B\cos\theta$ (the perpendicular component of the magnetic field). The angle θ is defined as the angle between the direction normal to substrate plane and the direction of the magnetic field. The data were measured at temperature of 2 K and were extracted from the magnetoresistance (MR) after subtracting the positive MR background.

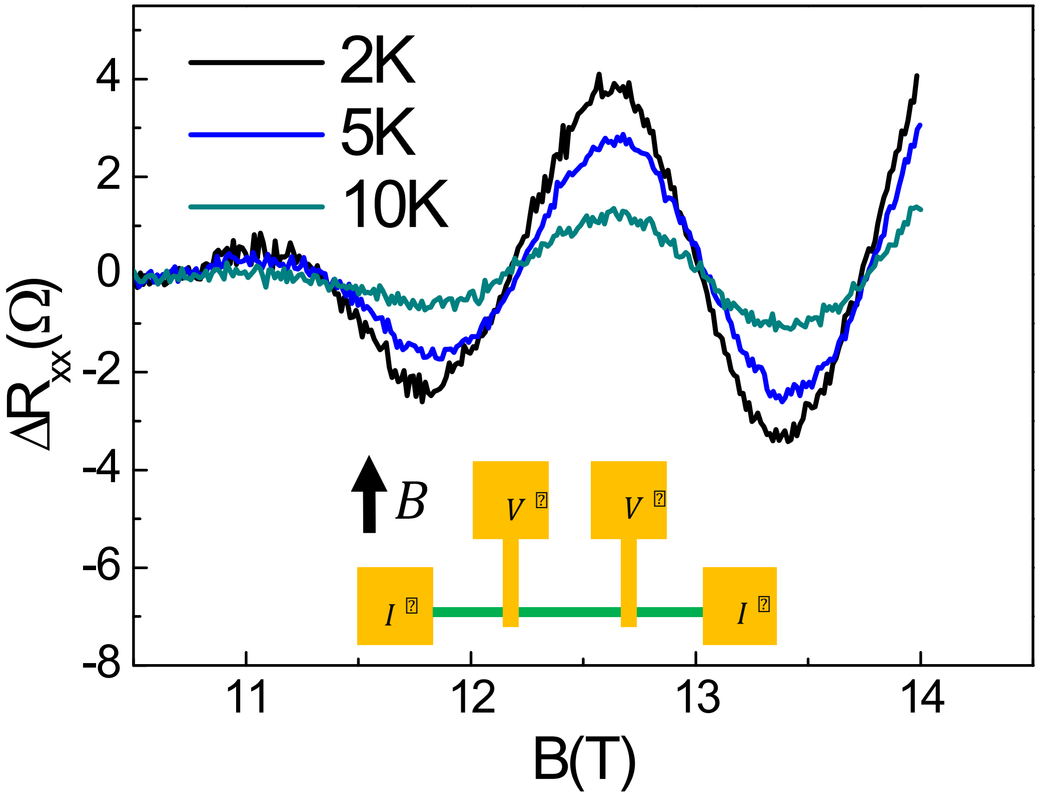

Supplementary Figure S3. The SdH oscillations measured at different temperatures and under an in-plane magnetic field that is perpendicular to the sidewall surfaces of the Bi_2Se_3 nanoribbon. Insert: the schematic geometry of the device referred to the direction of the magnetic field.

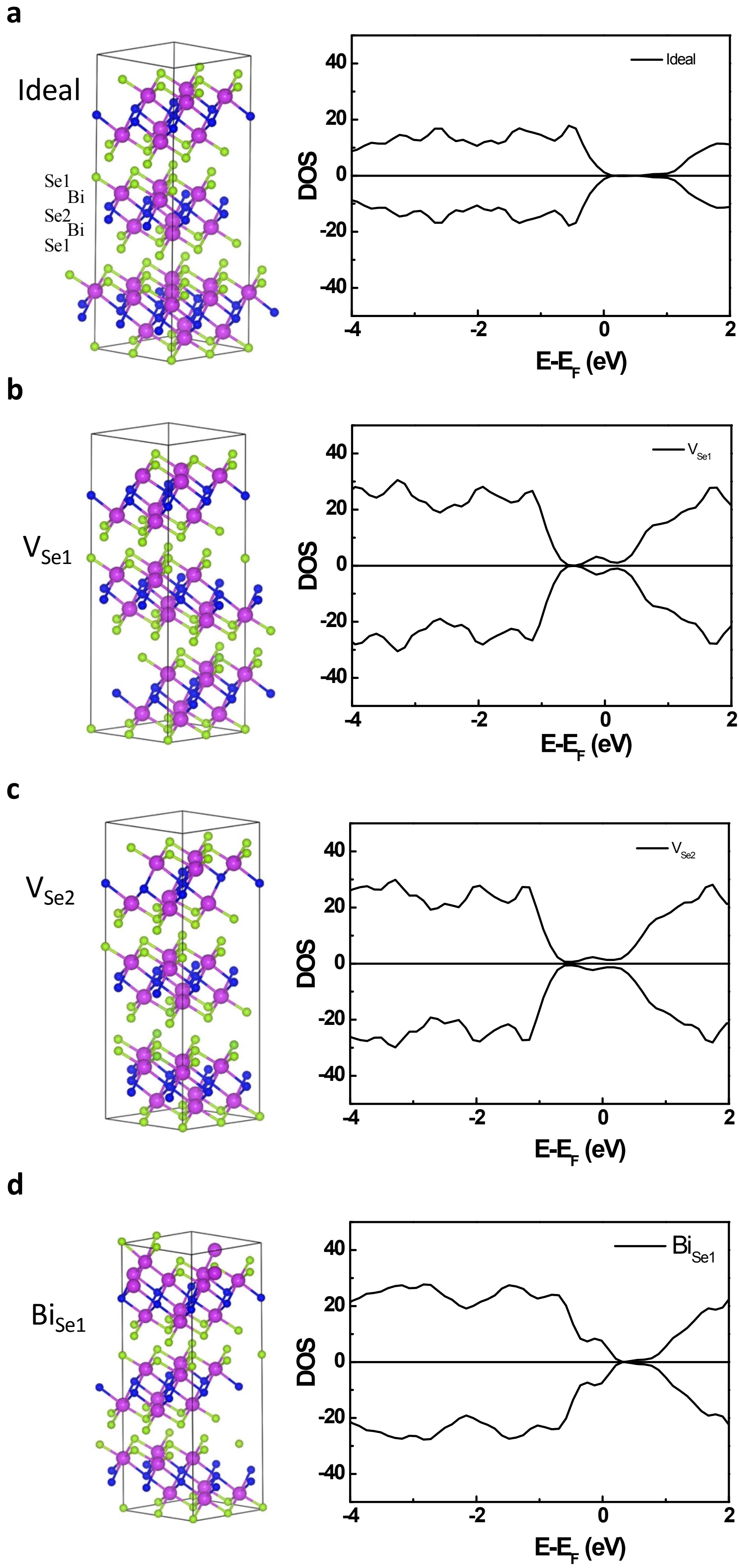
a
Ideal
Se1
Bi
Se2
Bi
Se1
Ideal
DOS
E-E$_F$ (eV)
b
V_{Se1}
V_{Se1}
DOS
E-E$_F$ (eV)
c
V_{Se2}
V_{Se2}
DOS
E-E$_F$ (eV)
d
Bi_{Se1}
Bi_{Se1}
DOS
E-E$_F$ (eV)

Supplementary Figure S4. Models (left panels) and the density of states (right panels) of the Bi_2Se_3 quintuple layers with (a) the ideal structure, (b) a Se1 vacancy, denoted as V_{Se1}, (c) a Se2 vacancy, denoted as V_{Se2}, and (d) a Se1 atom replaced by one Bi atom, denoted as a Bi_{Se1} anti-site defect.

For the DFT calculations, we consider a 2x2x1 supercell containing 60 atoms. The electronic structures were calculated by using the Vienna ab initio simulation package (VASP). We employed the projected augmented plane wave method. A cut-off energy of 400 eV has been used for geometry optimization and energy calculations. 1x1x1 and 4x4x1 Monkhorst–Pack k-point grids were applied to sample the Brillouin zone for geometry optimization and energy calculations, respectively. To study the effect of Se vacancy or the effect of anti-site defect, we removed one Se atom from the ideal Bi_2Se_3 structure or replaced a Se atom with one Bi atom and then performed a structure relaxation for the entire structure.

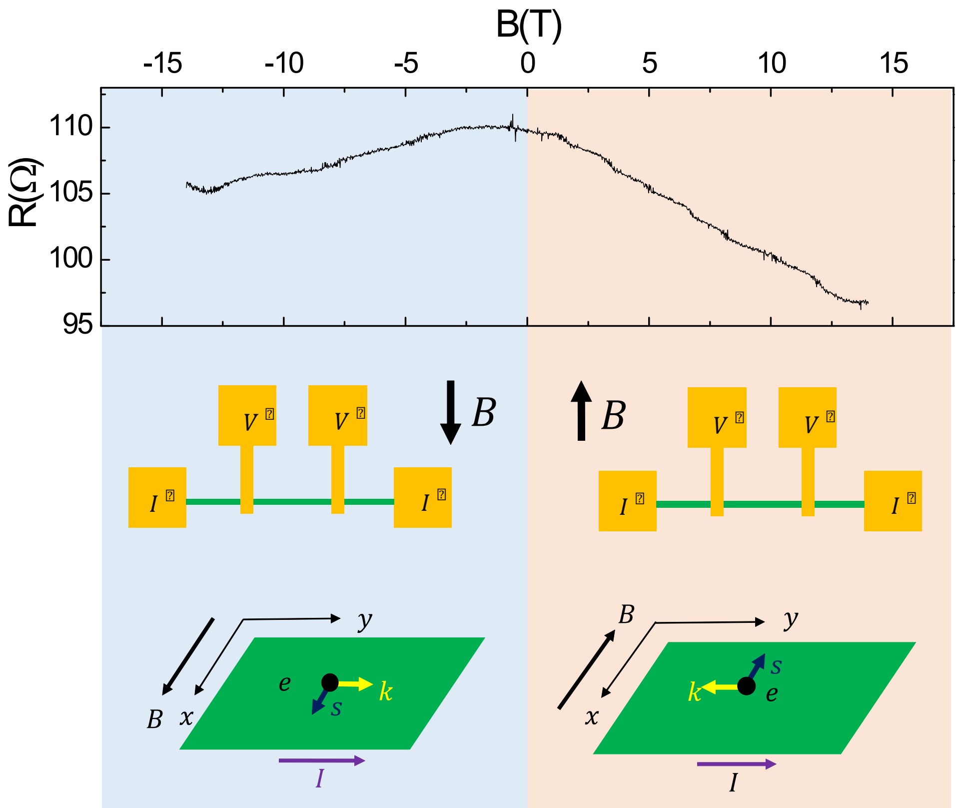

Supplementary Figure S5. The magnetoresistance of another similar sample measured under in-plane magnetic field that is perpendicular to the direction of the current. The magnetic field was swept from -14 to 14 T. The MR shows an asymmetry as changing the field polarity. The sketches illustrate the corresponding physical mechanism. The in-plane magnetic field will result in the spin-polarized surface states with the spin direction along with the magnetic field direction due to the magnetic field induced Dirac cone shift. Due to the spin-momentum locking, spin-polarized surface states will enhance or diminish the total conductance lying on whether the momentum direction of the spin-polarized surface states is antiparallel or parallel to the current direction.